# Chiral control of current transfer in molecules

Vered Ben-Moshe[1], David N. Beratan[2], Abraham Nitzan[1], and Spiros S. Skourtis[3]

[1] School of Chemistry, Tel Aviv University, Tel Aviv 69978, Israel

[2] Departments of Chemistry, Biochemistry and Physics, Duke University, Durham, NC 27708 USA

[3] Department of Physics, University of Cyprus, Nicosia 1678, Cyprus

## Abstract

Electron transmission through chiral molecules induced by circularly polarized light can be very different for mirror image structures. This behaviour is described in terms of *current transfer*: the transfer of both charge and momentum. We review recent theoretical developments on the theory of current transfer and discuss related experimental studies of electron transmission through chiral molecular structures adsorbed on surfaces.

## 1. Introduction

Charge transfer between donor and acceptor species mediated by a molecular bridge is of wide interest in chemistry, physics, biology and nanoscience [1-9]. The manipulation of charge transfer, electric currents, and magnetic moments in molecular junctions is of crucial importance in molecular electronics [10-12] and the development of attosecond laser pulses opens exciting new directions for the coherent control of electronic motion in atoms and molecules [13-15]. Indeed, novel experiments use attosecond laser pulses to probe and control ultrafast electronic dynamics in atoms and in small molecules [16-27]. Theoretical and computational studies indicate that an important application of attosecond laser pulses will be the generation of currents and induced magnetic moments in molecules. Circularly polarized attosecond laser pulses can be tailored to induce electric currents in linear [28-29] and ring-shaped molecules such as benzene and Mg-porphyrins [30-32]. Importantly, the laser-generated ring currents and their magnetic moments can be much larger than those generated by static magnetic fields [30-35]. Therefore, the development of theoretical and computational tools for the analysis of current propagation through molecules is central to the fields of molecular electronics and quantum control.

Experiments by Naaman, Waldeck and coworkers [36,37] show that the relative yield of electron transfer (ET) induced by circularly polarized light (CPL) through helical molecular structures adsorbed on surfaces depends on the relative handedness of the bridge and on the optical circular polarization, in spite of the identical underlying electronic energy spectra. Reversing the direction of the circular polarization or of the molecular handedness has similar effects on the yields, while the transmission of electrons generated by unpolarized light is not influenced by the handedness of the molecule.

Here, we review tight-binding models that account for the above mentioned ET yield asymmetries in the context of the more general phenomenon of *current transfer* [38,39]. Current transfer is charge transfer where the transferred charge carrier maintains at least some of its linear and/or angular momentum (phase). A recent photoemission experiment [40] demonstrated current transfer as a biased linear momentum distribution created on a Cu (100) surface was observed in the angular distribution of the photoemitted current.

As an application of current transfer theory, we examine bridge-mediated electron transport through chiral bridges and we demonstrate that the through-bridge transmission of an electronic state carrying angular momentuma or current is affected by the handedness of the bridge [38]. Our model explains the main features of the experimental data in [36,37] and provides a starting point for understanding how to control through-bridge transmission of electron phase, current, or angular momentum by manipulating the structure of the bridge [38,39].

**2.The transmission of polarized electrons through chiral molecular layers**

In Ref. 36, unpolarized and polarized photoelectrons are ejected from a Au substrate through Langmuir-Blodgett thin films of chiral molecules, L- or D- stearoyl-lysine, deposited on the substrate. The main observation of [36] is that the handedness of the layer determines the transmission of the photoelectrons generated by right (denoted $+$) versus left (denoted $-$) circularly polarized light. The molecular handedness does not affect the transmission of photoelectrons generated by unpolarized light ($0$). If $Y$ is the relative electron quantum yield scaled to unity for transmission of unpolarized electrons through an L layer, i.e., $Y[0,L]=1$, then the measured yields in [36] are $Y[0,D]=1.07$, $Y[+,L]=1.11$, $Y[+,D]=0.92$, $Y[-,L]=0.89$, and $Y[-,D]=1.21$ with errors of 1%-5%. Therefore, the average asymmetry in transmission through the L layer is $A[L]=\Delta Y\Phi[L]/\overline{Y}[L]=0.11$, where $\Delta Y[L]=Y[+,L]-Y[-,L]$ and $\overline{Y}[L]=\overline{Y}[+,L]+\overline{Y}[-,L]$, and for the D layer it is $A[D]=-0.14$. The asymmetry is of the order of 10%, and the yield asymmetry reverses sign when the handedness of the layer is switched.

In Ref. [37], monolayers of chirally substituted porphyrins are attached to Au electrodes and are immersed in an electrochemical cell. The Cys end of the molecules is attached to Au and the porphyrin group lies in solution. The porphyrin is excited with right- or left-circularly-polarized light, creating a polarized excited state. The porphyrin excited state is reduced by the Au. The observation in [37] is that the photocurrent induced by right-circularly polarized light differs from the photocurrent induced by left-circularly-polarized light, and this photocurrent asymmetry depends on the handedness of the molecular layer. In particular, for the L monolayer, the average photocurrent asymmetry is $A[L]=\Delta J[L]/\overline{J}[L]=-0.005\pm0.001$, and for the D monolayer it is $A[D]=0.004\pm0.002$.

Although the transmission asymmetry in the porphyrin system [37] is much lower than the asymmetry in the photoelectron transmission experiment [36], it is surprising that both experiments produce a transmission asymmetry, and that the effect on transmission of reversing the bridge handedness is equivalent to the effect of reversing the polarization of the CPL.

Photoelectrons generated by CPL carry total angular momentum polarization. We propose that the yield asymmetry obseved in [36] arises from the change in the orbital angular momentum polarization of the photoelectrons induced by the reversal of the exciting light's polarization [38]. Similarly, the photocurrent asymmetry observed in the porphyrin system [37] arises from the change in the orbital angular momentum of the photogenerated hole.[1] The difference in asymmetry magnitudes in the two experiments is attributed to a difference in bridge energetics relative to the energy of the photoelectrons (the weak effect in Ref. [37] is due to electron transmission via a tunneling mechanism).

**3.Time dependent current transport analysis**

A standard model for electron transfer in donor (D)-bridge(B)-acceptor(A) systems describes the donor, bridge, and acceptor species as tight-binding chains [2-9]. The corresponding Hamiltonian is: $\hat{H} = \hat{H}_D + \hat{H}_A + \hat{H}_B + \hat{V}_{BA} + \hat{V}_{BD}$, where

$$H_K = \sum_{j_K \in K} E_{j_K}^{(K)} \left| j_K \right\rangle \left\langle j_K \right| + \sum_{j_K \in K} V_{j_K, j_{K+1}}^{(K)} \left| j_K \right\rangle \left\langle j_K + 1 \right| \; ; \quad K = D, A, B \qquad (1)$$

and

$$V_{KK'} = \sum_{j_K \in K, j_{K'} \in K'} \sum V_{j_K, j_{K'}}^{(K,K')} \left| j_K \right\rangle \left\langle j_{K'} \right| \; ; \qquad (K, K') = (D, B) \; or \; (B, A) \qquad (2)$$

$\hat{H}_D$, $\hat{H}_B$, and $\hat{H}_A$ are the Hamiltonians of D, B and A. $\hat{V}_{BD}$ and $\hat{V}_{BA}$ describe the D-B and B-A interactions. We will discuss models where each of the D, B and A moieties have identical site energies and inter-site couplings, and where all D-B, (A-B) site pairs have identical couplings: $\alpha_K = E_{j_K}^{(K)}$; $\beta_K = V_{j_K, j_K+1}^{(K,K)}$ ; $V_{KK'} = V_{j_K, j_{K'}}^{(K,K')}$ [38,39].

Consider a tight-binding model for a structure with a donor ring, a helical

[1] Au photoelectrons are spin polarized due to the high spin-orbit coupling of the metal. Therefore, an alternative mechanism for the transmission asymmetry obseved in [36] could be based on changes in the photoelectron spin angular momentum. We do not attribute the yield assymetry to spin polarization because the stearoyl-lysine monolayers in [36] contain only low atomic number atoms that do not scatter spin.

bridge, and a model acceptor. (Fig. 1a). In comparison to the system studied in [37], the ring represents the porphyrin moiety, the helical bridge the peptidic linker and the single atom the gold contact electrode. The model in Fig. 1a is also applicable to the photoelectron experiment [36] in the sense that it incorporates the handedness of the stearoyl-lysine multilayer and the orbital polarization of the incoming (initial) electrons.

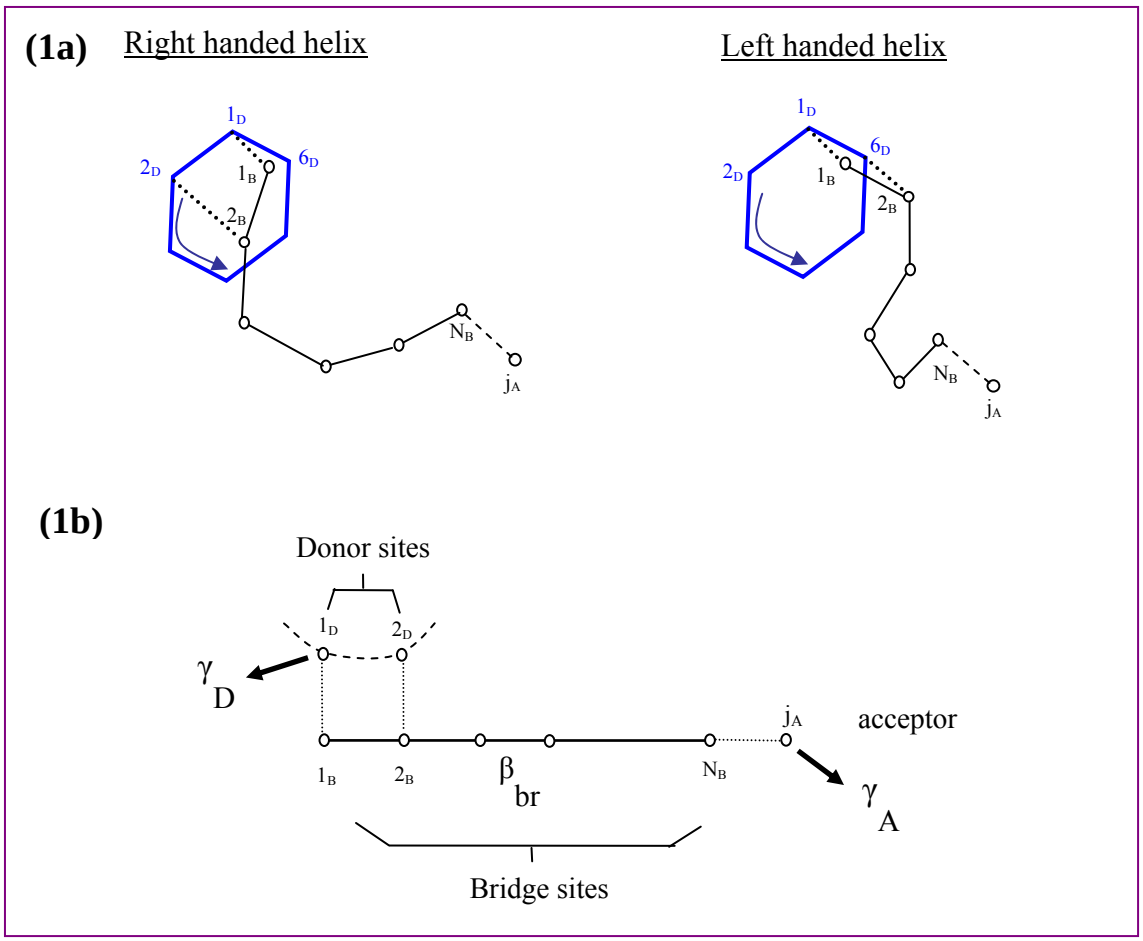


**Figure 1 (a)** Tight-binding donor–bridge-acceptor model where the donor moiety is a ring (sites $j_D$), the bridge is a right- or left-handed helical chain ($j_B$), and the acceptor ($j_A$) is an atom connected to the end of the bridge. **(b)** Simplified representation of the model that emphasizes the different ring-to-bridge tight-binding couplings for left- and right-handed helices. The arrows indicate population relaxation rates for donor and acceptor sites.

For the system in Fig. 1a, we assume that excitation induced by the circularly-polarized light produces a Bloch type state on the donor

$$\left|M_D\right\rangle = \frac{1}{\sqrt{N_D}} \sum_{j_D=1}^{N_D} \exp[i(j_D - 1)k_{M_D} a] \left|j_D\right\rangle, \quad k_{M_D} = 2\pi M_D / (aN_D) \qquad (3)$$

($N_D = 6$). Since coupling between D and B is assumed to be negligible among all but the nearest two sites of D and B, the bridge-coupled fragment of the $\left|M_D\right\rangle$ state is

$\left(\left|1_D\right\rangle + \exp[ik_{M_D}a]\left|2_D\right\rangle\right)/\sqrt{6}$ for the right-handed helical bridge and $\left(\left|1_D\right\rangle + \exp[-ik_{M_D}a]\left|6_D\right\rangle\right)/\sqrt{6}$ for the left-handed bridge. Reversing the bridge handedness is equivalent to reversing the current direction $\left(M_D \to -M_D\right)$. Indeed, this equal footing for bridge handedness and for the polarization of the excited states is consistent with the ET yields reported in Refs. [36,37].

We use a simplified version of the model in Fig. 1a to examine the effect of donor-current direction reversal on the electron-transfer yield following initial excitation of donor states $\left|M_D\right\rangle$ [38] that captures the physics of the electron transmission asymmetry reported in Refs. [36,37] (Fig. 1b). We represent the opposite initial circular currents on the donor by the initial states

$$\left|\phi_{in}\right\rangle = \frac{1}{\sqrt{2}}\left(\left|1_D\right\rangle + e^{i\theta}\left|2_D\right\rangle\right); \quad \left|\phi_{in}^{*}\right\rangle = \frac{1}{\sqrt{2}}\left(\left|1_D\right\rangle + e^{-i\theta}\left|2_D\right\rangle\right) \tag{4}$$

(the phase $\theta$ can be thought of as $k_{M_D}a$, but is not restricted to this value, and we have changed the normalization of the state). In addition, we assume that $\left|1_D\right\rangle$ in $\left|\phi_{in}\right\rangle$ is characterized by a finite lifetime $\hbar/\gamma_D$ and that the electron-transfer signal is associated with the decay of the acceptor state $\left|j_A\right\rangle$ with rate $\hbar/\gamma_A$. These population relaxations are described by replacing $E_{j_K}$ by $E_{j_K} - i\left((1/2)\gamma_K\right)$ in Eq. (1) for the corresponding donor and acceptor sites, i.e., $\left\langle j_K\left|\hat{H}\right|j_K\right\rangle = E_{j_K}^{(K)} - i(1/2)\gamma_K$ , $K = D, A$.

Starting from a given initial state $\left|\phi_{in}\right\rangle$, the probability that the acceptor state $\left|j_A\right\rangle$ is populated at time $t$ is $P_{j_A,in}(t) = \left|\langle j_A \mid e^{-i\hat{H}t/\hbar} \mid \phi_{in}\rangle\right|^2$ ($\hat{H}$ is the (non-hermitian) Hamiltonian of Eq. (1). The Hamiltonian has site-energies $E_j - i\left((1/2)\gamma_j\right)$ . The probability can be computed in terms of the right and left eigenvectors, $\left|X_q^{(R)}\right\rangle$ and $\left\langle X_q^{(L)}\right|$ of $\hat{H}$, and the corresponding eigenvalues, $\mathcal{E}_q = \varepsilon_q - i\Gamma_q/2$ ($\Gamma_q > 0$):

$$\langle j_A \mid e^{-i\hat{H}t/\hbar} \mid \phi_{in}\rangle = \sum_{q=1}^{N} \mathrm{R}_{j_A,in}^{(q)}\ e^{-i\mathcal{E}_q\, t/\hbar}; \quad R_{j_A,in}^{(q)} = \left\langle j_A \mid X_q^{(R)}\right\rangle\left\langle X_q^{(L)} \mid \phi_{in}\right\rangle \tag{5}$$

(N is the total number of sites in the DBA system). The yield of the irreversible flux out of the acceptor is

$$Y(in) = \gamma_A \int_0^\infty dt \sum_{j_A} P_{j_A,in}(t) \tag{6}$$

The circularly polarized excitation ($|M_D\rangle$ vs. $|-M_D\rangle$) produces asymmetry:

$$A \equiv \frac{Y(M_D) - Y(-M_D)}{Y(M_D) + Y(-M_D)}, \tag{7}$$

Reversing the handedness of the bridge produces the same asymmetry. In the model of Fig 1b, $|M_D\rangle$ corresponds to $|\phi_{in}\rangle$ in Eq. 4 and $|-M_D\rangle$ to $|\phi_{in}^*\rangle$.

*Dephasing.*

The current transfer described here is a coherent phenomenon, sensitive to dephasing. To investigate environmental dephasing effects, we incorporate additional relaxation of coherences in the site representation of the Liouville equation for the system's density matrix $\tilde{\rho}$:

$$i\hbar \frac{d}{dt}\rho_{j,l}(t) = \sum_k \left[ H_{j,k}\rho_{k,l}(t) - \rho_{j,k}(t)H_{kl} \right] - \left\{ i\left(\gamma_j/2 + \gamma_l/2\right) + i\gamma_{jl} \right\} \rho_{j,l}(t), \tag{8}$$

Here, as above, the population relaxation rates $\gamma_j$ are non-zero only for donor and acceptor states. The probability $P_{j_A,in}(t) = \rho_{j_A,j_A}(t)$ needed in Eq. (6) is obtained from Eq. (8) using the initial condition $\hat{\rho}(t=0) = |\phi_{in}\rangle\langle\phi_{in}|$.

In the model of Fig 1b, all bridge site-energies are taken equal ($E_{j_B}^{(B)} = \alpha_B$), and similarly for the bridge nearest-neighbor couplings ($V_{j_B,j_B+1}^{(B,B)} = \beta_B$), and for the donor-bridge and acceptor-bridge couplings ($V_{1_D,1_B}^{(D,B)} = V_{2_D,2_B}^{(D,B)} = V_{N_B,j_A}^{(B,A)} \equiv V$). The complex energies of the donor sites ($1_D$ and $2_D$) and of the acceptor site ($j_A$) are taken to be $\alpha_D - i(1/2)\gamma_D$, $\alpha_D$, and $\alpha_A - i(1/2)\gamma_A$ (where $\alpha_D = \alpha_A$). Using Eqs. (6) and (7), this leads to

$$\int_0^\infty dt\, P_{j_A,in}(t) = \hbar \sum_{q=1}^N \frac{\left|\mathrm{R}_{j_A,in}^{(q)}\right|^2}{2\Gamma_q} + 2\hbar \sum_{q>q'}^N \mathrm{Im}\left\{ \frac{\mathrm{R}_{j_A,in}^{(q)} \left\{\mathrm{R}_{j_A,in}^{(q')}\right\}^*}{(\varepsilon_q - \varepsilon_{q'}) - i(\Gamma_q + \Gamma_{q'})} \right\}, \tag{9}$$

where $\mathcal{E}_q = \varepsilon_q - i\Gamma_q$ are the eigenenergies of the dissipative Hamiltonian, and $R_{fi,in}^{(q)} = \langle \phi_{fi} | X_q^{(R)} \rangle \langle X_q^{(L)} | \phi_{in} \rangle$. We solve Eq. (8) using $\hat{\rho}(t=0) = |\phi_{in}\rangle\langle\phi_{in}|$ or $|\phi_{in}^*\rangle\langle\phi_{in}^*|$ with $\gamma_{D(A)}/2 > 0$. Donor coherence relaxation is accounted for by taking $\gamma_{12} > 0$. We calculate the yield asymmetry using Eqs. (6) and (7).

In Fig. 2, we show the computed asymmetry A, Eq. (7) vs. the bridge length for resonant ($\alpha_B - \alpha_{D(A)} = 0$) and non-resonant ($\alpha_B - \alpha_{D(A)} = 3\,\mathrm{eV}$) bridges, for different donor and acceptor lifetimes, and in the absence of dephasing. The parameters used (donor and acceptor lifetimes in the range 3-30 fs and tight-binding couplings of order 1 eV) are reasonable for nonfluorescing excited electronic states with covalent intersite bonding. It should be emphasized, however, that other values of lifetimes and couplings will generate yield asymmetries. The yield asymmetry becomes independent of length for long bridges and is about an order of magnitude larger in the resonant case compared to the off-resonant case. $\mathcal{A}$ increases with decreasing donor and acceptor lifetimes in both resonant and off-resonant cases. More detailed findings indicate that the donor lifetime effect is dominant in this regard. For parameters in the range studied, and for sufficiently short donor lifetimes, effects are found of the order observed in the experiments (~10% for a resonant bridge [36] and <1% in the off-resonant case [37]). The asymmetry disappears for extremely short donor (acceptor) lifetimes.

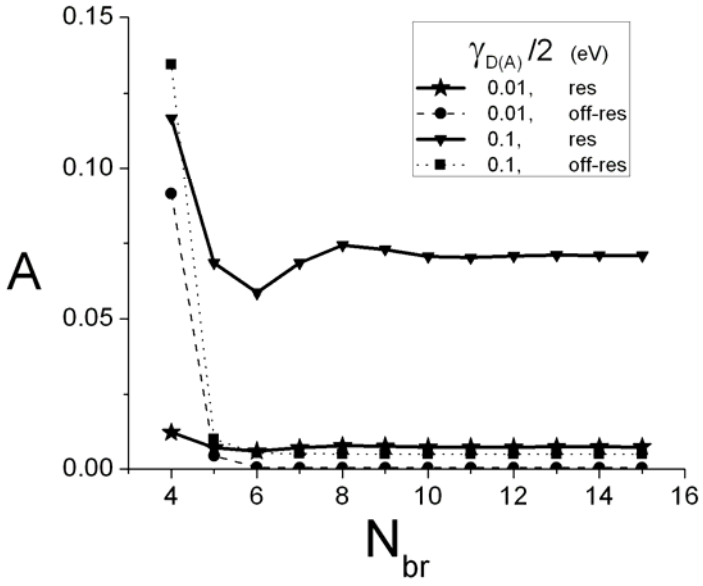


**Figure 2**. Yield asymmetry vs. bridge length $N_{br}$, for the model of Fig. 1b, for resonant ($\alpha_B - \alpha_{D(A)} = 0$, squares, solid lines), and off-resonant ($\alpha_B - \alpha_{D(A)} = 3\,\mathrm{eV}$, circles, dashed lines) bridges. Black and blue correspond to $\gamma_D = \gamma_A = 0.02$ eV, and $\gamma_D = \gamma_A = 0.2$ eV, respectively. The other parameters are $\beta_B = 0.5$ eV, $V = 1.0$ eV, $\theta = \pi/4$ and $\gamma_{i,j} = 0$ for $i \neq j$.

Fig. 3 shows the effect of dynamic interactions with the thermal environment, in particular the effect of decoherence arising from nuclear motion. Fig. 4 shows the effect of

donor decoherence. The figure plots $\mathcal{A}$ vs. $\gamma_{12}$ for resonant and non-resonant bridges. It should be noted that, although increasing decoherence eventually destroys the asymmetry, the loss of yield asymmetry only arises for unphysical large $\gamma_{12}$ for the resonant-bridge case. Similar results are obtained in the presence of bridge decoherence.

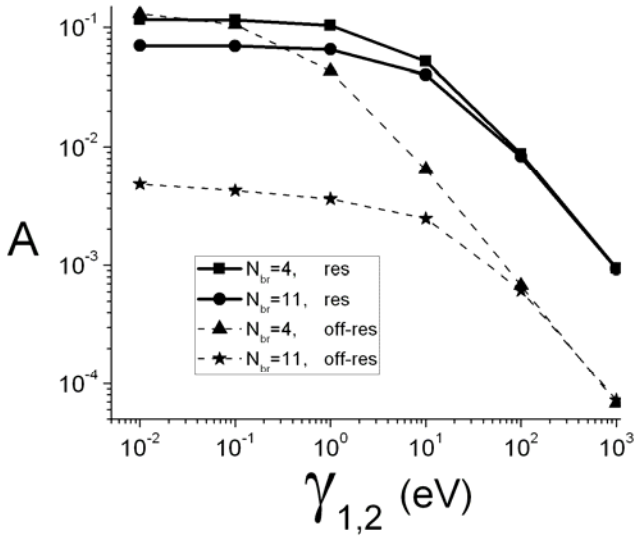


**Figure 3**. The yield asymmetry vs. donor decoherence (model of Fig. 1b) for resonant and non-resonant bridges of different lengths. Parameters used (except $\gamma_{12}$) are the same as in Fig. 2 with $\gamma_D = \gamma_A = 0.2$ eV. The behavior of the asymmetry with respect to donor decoherence shown above is obtained for a wide range of values of $\gamma_{D(A)}$.

The simple model of Fig. 1b is not expected to reproduce the experimental results of 6 and 7 quantitatively, but it does yield three distinctive and robust features that characterize our model in a relatively large range of system parameters. These include an independence of bridge length for long molecular bridges, an asymmetry that increases as donor lifetime shortens (within physically reasonable values), and an asymmetry that persists in the presence of decoherence. For a reasonable range of system parameters, the calculated asymmetry is the same order as that seen experimentally for reversed circular polarization. Importantly, the resilience of this asymmetry to decoherence rationalizes the observed behavior in condensed thermal environments. Introduction of site-energy and nearest-neighbor coupling disorder in the Hamiltonian can reduce the magnitude of the asymmetry for resonant transport. Indeed, the experiments of Ref. [36] find that the asymmetry disappears when, in a molecular layer of a given handedness, as few as 1% of the molecules are substituted by molecules of the opposite handedness.

The model of Fig. 1b does not rely on the bridge's chiral structure, but rather on

the nature of the donor excitation and the proximity effects (derived from the chiral structure) that determine the nature of the donor-bridge coupling. These proximity effects are apparent in chiral molecules and nanostructures. We suggest that electron donor – bridge –acceptor devices could carry electron phase information by optically creating angular-momentum-polarized electron states and by manipulating the bridge's connectivity to the donor and acceptor. Semiconductor nanoparticles linked by DNA or helical polypeptides are particularly promising [41]. In many of these imagined device systems, the experiments involve generation and observation of steady state currents. It is thus important to extend current-transfer theory to the steady-state regime, as we describe next [39].

**4. Steady-state transport analysis**

In the previous section, we examined the time evolution that follows excitation of a ring current in the donor (Fig. 1a). The ring state $|M_D\rangle$ is an eigenstate of the donor moiety with the eigenvalue $E\left(K_{M_D}\right)=\alpha_D+2\beta\cos\left(K_{M_D}a\right)$ and with time evolution $|M_D\rangle e^{-iE\left(K_{M_D}\right)t/\hbar}$, where $K_{M_D}=2\pi M_D/\left(aN_D\right)$ is quantized. Hence, the injection energy of the electron was determined by the energy of a photo-prepared donor state. We now examine a case where the donor (D) is a wire that is coupled to an acceptor (A) wire directly or through a bridging (B) wire. The D wire is restricted to carry a constant current $J_D$ and we explore the steady state response of the rest of the system. All charge carriers in the system originates from this wire. The injection energy can now take any value within the D-wire energy band.

The models displayed in Figs. 4a and b that respectively represent the direct (DA) and the bridge-mediated (DBA) systems correspond to a tight-binding Hamiltonian with nearest neighbour couplings indicated by the arrows connecting different sites. In the DA system we investigate the current transfer from D and A through couplings between $N_{DA}$ pairs of neighbouring atoms on different wires. In the DBA system we examine the charge transfer from D to A through B. In this case, $N_{DB}$, $N_{BA}$ and $N_B$ denote, respectively, the number of site pairs connecting the wires D and B, the number of sites on B between these coupling regions.

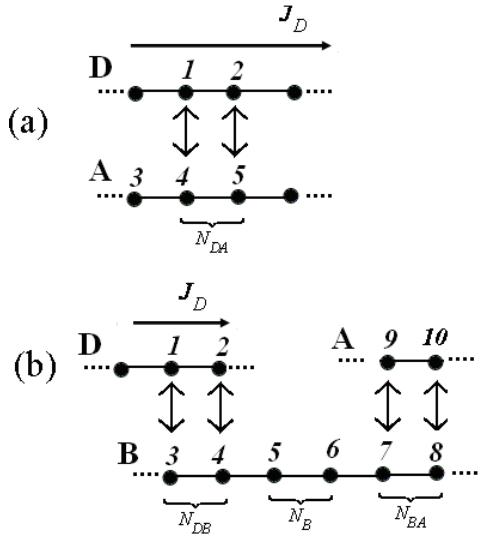


**Figure** 4. Simple models of current transfer. In both models a driving current $J_D$ in wire D is transferred to wire A. In (a) the transfer is direct while in (b) it is mediated by a "bridge" wire B.

As in the time-dependent case, the relevant sites on the driver wire are those directly coupled to the A wire of the DA system or to the B wire of the DBA system (e.g., sites 1 and 2 of Figs. 4a and b). The driving conditions on these sites are represented by the Bloch wave

$$\left|\psi_D(t)\right\rangle = c_1(t)\left|1\right\rangle + c_2(t)\left|2\right\rangle = \left(\overline{c}_1\left|1\right\rangle + \overline{c}_2\left|2\right\rangle\right)e^{-(i/\hbar)Et} \tag{10a}$$

$$\overline{c}_2 = \overline{c}_1 e^{ik_D a} \tag{10b}$$

where $a$ is the lattice constant and $k_D$ is the wave vector of the D wire that is related to the injected electron energy $E$ by the dispersion relation

$$E = \alpha_D + 2\beta_D \cos(k_D a) \tag{11}$$

The time dependent Schrödinger equation of the Hamiltonian in Eqs. (1), (2) of the DBA system (or its equivalent for the DA system) in the site representation is

$$\hbar\frac{dc_n}{dt} = -iE_n c_n - i\sum_\alpha V_{n,\alpha} c_\alpha \tag{12}$$

where $\alpha$ sums over all sites that couple with coupling element $V_{n,\alpha}$ to site $n$.

The infinite extent of the bridge and acceptor wires in Figs. 4a and b provides an effective dissipation mechanism. This mechanism allows the systems to reach a steady state that yields solutions at long times of the form

$$c_n(t) = \overline{c}_n e^{-iEt/\hbar} \tag{13}$$

for all the amplitudes of the A and B wires. Inserting Eq. (13) into Eq. (12) leads to a set of equations for the steady state amplitudes $\bar{c}_n$

$$0 = -i\left(E_n - E\right)\bar{c}_n - i\sum_{\alpha} V_{n,\alpha}\bar{c}_\alpha \tag{14}$$

Eqs. (14) define the steady-state wavefunction of the DBA (or DA) system, $\Psi(t) = \sum_{n\in B,A} c_n(t)|n\rangle$. Terms involving coefficients on the driving wire appear in the inhomogeneous part of these equations.

In the time-dependent case (section 3), this was achieved by assigning (real and positive) population-relaxation rates $\gamma_j$ to some sites by replacing $E_j$ by $E_j - (1/2)\gamma_j$ for these sites in Eqs. (1), (2) and (12). In the steady-state approach, the infinite set of equations (12) and (13) becomes finite by separating the overall system into interior and exterior parts, and accounting for the effect of the latter on the dynamics of the former by introducing energy-dependent "self energy" term. In particular, in Fig. 4a, the effect of an exterior part defined as the infinite linear chain extending right to the cut-off site 5 on A is provided by modifying Eq. (14)

$$0 = -i\left(E_A + \Sigma_A(E) - E\right)\bar{c}_5 - i\beta_A\bar{c}_4 - iV_{AD}\bar{c}_2 \tag{15}$$

where $\Sigma_A(E)$ is the self energy of a one-dimensional tight binding wire, with real and imaginary parts $\Lambda_A(E)$ and $-i\left(\gamma_A(E)/2\right)$ respectively,

$$\Sigma_K(E) = \frac{E - E_K - \sqrt{(E-E_K)^2 - 4\beta_K{}^2}}{2} \equiv \Lambda_K(E) - \frac{i}{2}\gamma_K(E) \qquad K = B, A \tag{16}$$

The finite set of steady state equations for the model in 4b, for example, is

$$\begin{aligned}
0 &= -i\left(E_B + \Sigma_B(E) - E\right)\bar{c}_3 - i\beta_B\bar{c}_4 - iV_{BD}\bar{c}_1 \\
0 &= -i\left(E_B - E\right)\bar{c}_4 - i\beta_B\bar{c}_3 - i\beta_B\bar{c}_5 - iV_{BD}\bar{c}_2 \\
0 &= -i\left(E_B - E\right)\bar{c}_5 - i\beta_B\bar{c}_4 - i\beta_B\bar{c}_6 \\
0 &= -i\left(E_B - E\right)\bar{c}_6 - i\beta_B\bar{c}_5 - i\beta_B\bar{c}_7 \\
0 &= -i\left(E_B - E\right)\bar{c}_7 - i\beta_B\bar{c}_6 - i\beta_B\bar{c}_8 - iV_{BA}\bar{c}_9 \\
0 &= -i\left(E_B + \Sigma_B(E) - E\right)\bar{c}_8 - i\beta_B\bar{c}_7 - iV_{BA}\bar{c}_{10} \\
0 &= -i\left(E_A + \Sigma_A(E) - E\right)\bar{c}_9 - i\beta_A\bar{c}_{10} - iV_{AB}\bar{c}_7 \\
0 &= -i\left(E_A + \Sigma_A(E) - E\right)\bar{c}_{10} - i\beta_A\bar{c}_9 - iV_{AB}\bar{c}_8
\end{aligned} \tag{17}$$

or

$$\mathbf{Mc} = \mathbf{d} \tag{18}$$

where **c** is the column vector transpose$\left(\overline{c}_3, \overline{c}_4, \overline{c}_5, \overline{c}_6, \overline{c}_7, \overline{c}_8, \overline{c}_9, \overline{c}_{10}\right)$, **M** is the matrix multiplying this vector in Eq. (17), and **d** is the driving vector transpose$\left(iV_{BD}\overline{c}_1, iV_{BD}\overline{c}_2, 0, 0, 0, 0, 0, 0\right)$.

Inverting **M** in Eq. (18) and using Eq. (13) produces all of the steady state coefficients in terms of the steady state amplitude $\overline{c}_1$. In the next section, we use these coefficients to evaluate all of the currents in the system in terms of the driving current $J_D$.

## 5. Steady-state currents and asymmetry factors

The steady state (SS) equation for the population on site *n* derived from Eqs. (12)-(14) with $E_n + \Sigma_n(E)$ replacing $E_n$ when *n* is an edge site is

$$0 = \left(\frac{d\left|c_n(t)\right|^2}{dt}\right)_{SS} = \sum_\alpha \frac{2V_{n,\alpha}}{\hbar}\mathrm{Im}\left(c_\alpha c_n^*\right) - \frac{\gamma_n(E)}{\hbar}\left|c_n\right|^2 \delta_{n,edge} \tag{19}$$

The sum in Eq. (19) runs over all sites coupled to site *n* with coupling $V_{n,\alpha}$ ($V_{n,\alpha} = \beta_K$ if *n* and $\alpha$ are nearest neighbours (NN) on the same wire *K*; $V_{n,\alpha} = V_{K,K'}$ if these sites are NN belonging to different wires *K* and *K'*). $\gamma_n(E) = -2\,\mathrm{Im}\,\Sigma_n(E)$ contributes only if site *n* is an edge site on A ($\gamma_n = \gamma_A$) or B ($\gamma_n = \gamma_B$).

Eq. (19) implies that the net current from site $n-1$ to site *n* on a wire *K* is

$$J_{K(n-1\to n)} = \frac{2\beta_K}{\hbar}\mathrm{Im}\left(c_{n-1}c_n^*\right) \tag{20}$$

and the current out of the system at the edge site *n* on *K* is

$$J_{K(n\to out)} = \frac{\gamma_K(E)}{\hbar}\left|c_n\right|^2 \tag{21}$$

We denote current from left to right as positive. In addition, positive assignments are also chosen for the D → A, D → B and B → A directions.

The currents out of the A wire to the right and to the left in the DA system are

$$J_A^{right} = \frac{2\beta_A}{\hbar}\mathrm{Im}\left(c_{eright-1}c_{eright}^*\right) = \frac{\Gamma_A(E)}{\hbar}\left|c_{eright}\right|^2 \tag{22}$$

$$J_A^{left} = \frac{2\beta_A}{\hbar}\mathrm{Im}\left(c_{eleft+1}c_{eleft}^*\right) = \frac{\Gamma_A(E)}{\hbar}\left|c_{eleft}\right|^2 \tag{23}$$

where *eleft* and *eright* denote respectively the left and right edge sites in the interior part

of the A wire. Symmetry requires that $J_A^{right}(k_D) = J_A^{left}(-k_D)$. A non-zero current asymmetry factor for the DA model of Fig. 4a

$$A_1 = \frac{J_A^{left} - J_A^{right}}{J_A^{left} + J_A^{right}} \tag{24}$$

denotes current transfer from D to A.

For the DBA model in Fig. 4b, we consider the total charge transmitted to the A wire and measured by $J_A^{total} \equiv J_A^{left} + J_A^{right}$ with regard to the direction of the driving current. Hence, in the case of the DBA system, we examine the following current asymmetric factor

$$A_2 = \frac{J_A^{total}(-k_D) - J_A^{total}(k_D)}{J_A^{total}(-k_D) + J_A^{total}(k_D)} \tag{25}$$

that is directly related to the observations in Refs. [36,37].

The following normalized differences are also of use

$$\overline{A_1} = \frac{J_A^{left} - J_A^{right}}{|J_D|} \tag{26}$$

$$\overline{A_2} \equiv \frac{J_A^{total}(-k_D) - J_A^{total}(k_D)}{|J_D|} \tag{27}$$

where $J_D$ is the donor (driving) current.

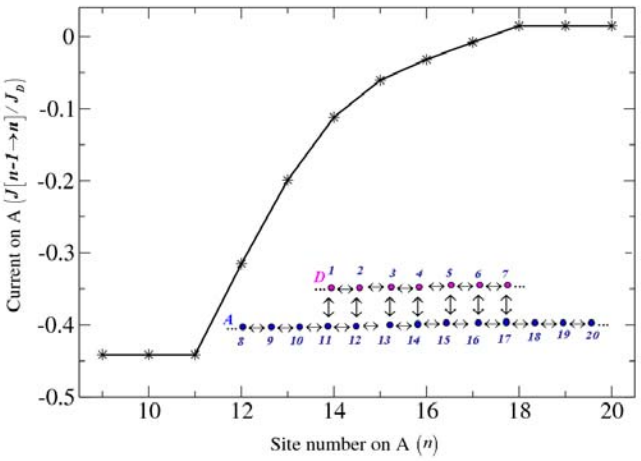


**Figure** 5. Wire A current distribution for the DA system shown in the inset, characterized by 7-sites coupling between the D and A wires. Here, $|J_D| = 1$, $E_D = E_A = 0$, $\beta_D = \beta_A = 0.1$, $V_{DA} = 0.01$ and

the injection energy is $E=-0.17$. The phase $k_D a=\arccos\left[\left(E-E_D\right)/2\beta_D\right]$ is taken positive, implying that the driving current goes from left to right.

The current distribution is shown in Fig. 5 for the A wire of the inset. Here and below, the coupling between the NN sites on each wire ($\beta_D, \beta_B$ and $\beta_A$) are chosen to be 0.1 and all other energy units are determined accordingly. The driving current on the D wire induces left and right going currents at the left and right edge sites, respectively, on the A wire. The current transfer character of the process is expressed by the larger leftward current with respect to the rightward current on A displayed in Fig. 5.

Fig. 6 shows the current asymmetry factor $\mathcal{A}_1$ of Eq. (24), displayed vs. the number of links, $N_{DA}$, connecting the D and A wires in a DA system of Fig. 4a. The inset shows the same data, presented in terms of the normalized difference $\overline{A_1}$ of Eq. (26), plotted vs. $N_{DA}$. Fig. 7 shows the corresponding property $\overline{A_2}$ of Eq. (25) for the DBA system of Fig. 4b displayed against the number of links, $N_{DB}$ connecting the D and B wires. The inset shows the same data, presented in terms of the normalized difference $\overline{A_2}$ of Eq. (27), plotted against $N_{DB}$. In the case that only one site couples directly to the D wire, no information about the direction of the electrons on the D wire is transferred to the A wire in either systems. Hence, in the case of the DA system $A_1=\overline{A_1}=0.0$ and in the case of the DBA system, $A_2=\overline{A_2}=0.0$. In both systems, asymmetry increases and then saturates near 1 (when the response current becomes nearly unidirectional) as the number of links to the D wire increases.

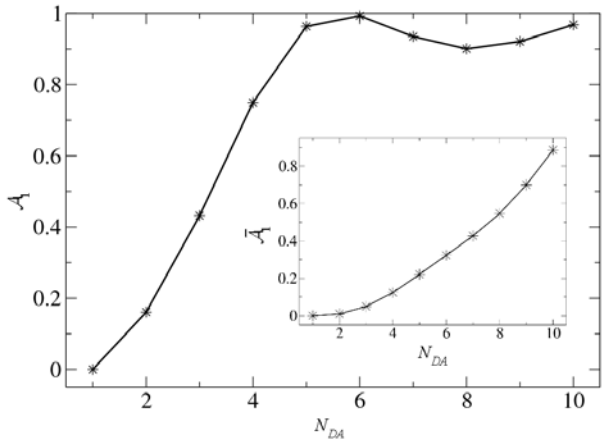


**Figure** 6. The current asymmetry factor $A_1$ as a function of the number of links, $N_{DA}$ connecting the D

and A wires in the DA system displayed in Fig. 4a. The inset shows the same data, presented in terms of $\overline{A_1}$ plotted as a function of $N_{DA}$. Parameters are similar to those in Fig. 5.

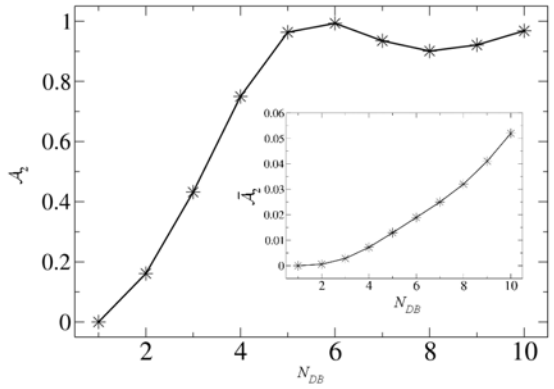


**Figure** 7. Current asymmetry $A_2$ as a function of the number of links $N_{DB}$ connecting the D and B wires in the DBA system displayed in Fig. 4b. The system parameters are $E_D = E_B = E_A = 0;\ \beta_D = \beta_B = \beta_A = 0.1,\ V_{DB} = V_{BA} = 0.01$, $N_{BA}$=2 and the injection energy is $E = -0.17$. The same data, presented as $\overline{A_2}$ vs $N_{DB}$ are shown in the inset.

Substantial current transfer asymmetry is indicated by the large asymmetry factors in Figs. 6-7 for both direct and bridge-assisted transfer. The calculated asymmetry factors are much smaller for short bridges. The steady-state scenario is different from the transient process considered in section 3 where, for short pulses, reflection does not set in appreciably during the process lifetime.

An important factor discussed in section 3 (Ref. [38]) is the energy dependence of current transfer. The results displayed in Figs. 5-7 correspond to resonance transmission in which site energies in all wires are equal $\left(E_D = E_B = E_A\right)$. The equivalent superexchange mechanism for non-resonant transfer, would be the DBA system where the site energies of the B ("bridge") wire are different from the site energies of the "donor" and "acceptor" wires, $E_B \neq E_D = E_A$. In the calculation below, we take $E_D = E_A = 0$, $\beta_D = \beta_A = \beta_B = 0.1$, an injection energy $E = -0.17$, and display the current transfer dependence on the B wire energy, $E_B$. The energy bands in these tight-binding wires range within $E_K \pm 2\beta_K$ ($K$=$D$, $B$, $A$). Hence, the non-resonant transfer sets in as $E_B$

decreases below $E_B = -0.37$ or increases above $E_B = 0.03$.

Fig. 8 shows the current-transfer process in the DBA system for the off-resonance regime, $E_B > 0.03$. In Fig. 8, the current transfer property decays quickly as we go into the off-resonance transfer regime. We find a strong exponential damping of the current transfer property expressed by the asymmetry factor $A_2$.

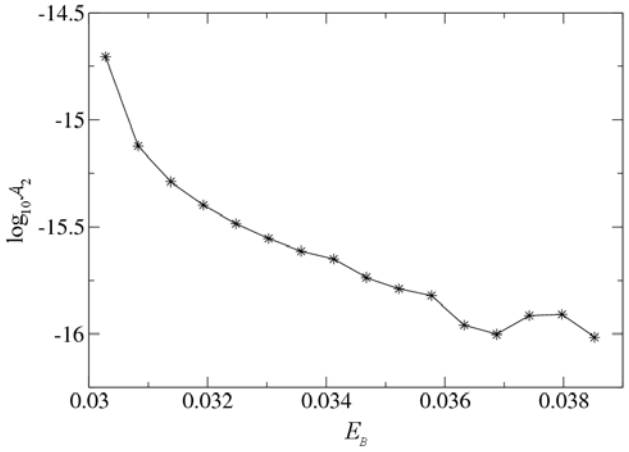


**Figure** 8. The current asymmetry factor $A_2$ as a function of the bridge site energy $E_B$ for the DBA system in the off-resonance regime, $E_B > 0.03$. The parameters used in this calculation are $E_D = E_A = 0$, $\beta_D = \beta_B = \beta_A = 0.1$, $V_{DB} = V_{BA} = 0.01$, $E = -0.17$, $N_{DB} = 3$, $N_B = 2$, $N_{BA} = 2$. Coarse grained averaging was used to reduce numerical errors that results from computing small differences between relatively large numbers.

## 6. Steady state current transfer in case of dephasing

As discussed in section 3, it is of interest to examine the effect of dephasing on the efficiency of current transfer. We assume that the driving wire D remains coherent (i.e. the Bloch wave holds, Eqs. (10)), and study the effect of dephasing on the "acceptor" (A) wire in the DA system and the "bridge" wire (B) in the DBA system. For this purpose, we shift from the local-site representation of the steady-state analysis to the density matrix (DM) representation and to the ensuing Liouville-space dynamics. Within the DM framework, we can study effects of “pure” dephasing in which non-diagonal elements of the DM are damped while the population (diagonal elements) dynamics is not affected.

The transition from the Schrödinger equation description, $i\hbar d|\Psi\rangle/dt = \hat{H}|\Psi\rangle$, of a closed quantum mechanical system to a Liouville space description, $i\hbar\, d\hat{\rho}/dt = \left[\hat{H}, \hat{\rho}\right]$ is useful. To explore dephasing effects in particular, the density matrix elements

$\rho_{nm} = c_n c_m^*$ of our tight-binding model in the site representation can be obtained using Eq. (12). We use Eq. (13) to deduce that, at steady state, $d\rho_{nm}/dt = 0$. Furthermore, population damping enters in the time evolution of diagonal density-matrix elements as $d\rho_{nn}/dt = ... - \gamma_n \rho_{nn}$ and in the corresponding equations for non-diagonal elements as $d\rho_{nm}/dt = ... - (1/2)(\gamma_n + \gamma_m)\rho_{nm}$ (section 3). This holds also in steady-state situations involving infinite wire systems, where apparent damping results from the imaginary part of the self energy of edge sites, as discussed in section 3, i.e. $d\rho_{nm}/dt = 0 = ... - (1/2)(\gamma_n(E) + \gamma_m(E))\rho_{nm}$.

We follow the procedure of Segal and Nitzan [42-43] to implement the driving conditions on the D wire in these steady-state Liouville equations [39]. We now describe results that show the effect of dephasing on current-transfer processes. In these results, we assigned dephasing rates $\gamma_n = \gamma$ to the $N_{DA}$ sites of the A wire that are linked to the D wire in the DA system (Fig. 4a) and to the $N_{DB} + N_B + N_{BA}$ sites on the B wire that connect between the D and A wires in the DBA system (Fig. 4b).

Fig. 13 shows the current transfer process in the presence of dephasing in the case of the DA and DBA systems, respectively. As observed above (section 3), while the current transfer efficiency drops with increasing $\gamma$, the effect persists up to relatively large values of the dephasing rate (of the order of other energetic parameters in the system such as NN coupling in the wires).

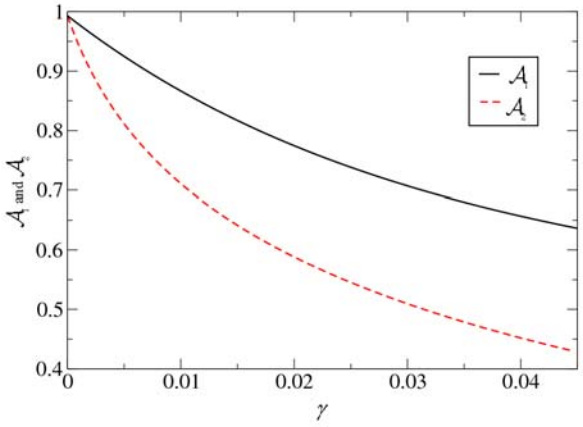


**Figure** 9. The current asymmetry factors $A_1$ and $A_2$ as a function of the dephasing rate $\gamma$. The black solid line is $A_1$ for a DA system (Fig. 4a) characterized by the parameters $N_{DA} = 6$, $V_{DA} = 0.01$. The phase

$k_D a = \arccos\left(\frac{E - E_D}{2\beta_D}\right)$ was taken positive, implying leftward driving current on the D wire. The red dashed line is $A_2$ for a DBA system (Fig. 4b) characterized by the parameters $N_{DB} = 6$, $N_B = 3$, $N_{BA} = 1$, $E_B = 0$, $\beta_B = 0.1$, $V_{DB} = V_{BA} = 0.01$. For both systems, $E_D = E_A = 0$, $\beta_D = \beta_A = 0.1$ and $E = -0.17$

## 7. Conclusions

Current transfer shifts both charge and momentum from donor to acceptor. We reviewed time-dependent [38] and steady-state [39] descriptions of current transfer through chiral bridges [36, 37]. In the tight-binding models, current transfer arises from coherent interferences between resonant or tunneling paths. This kind of interference has received attention in recent studies of molecular wires and nanodots [44].

In the models reviewed here, one-dimensional chains represent the donor (D), bridge (B) and acceptor (A) moieties. In the first model described here, this current is time dependent, and the time evolution of the system is computed. In the second model, this driving current is constant, and a steady-state current is computed.

In the time-dependent analysis, we address the yield asymmetry of the irreversible flux from the acceptor (A) wire for opposite directions of currents on D. This calculated yield-asymmetry peaks for short bridges and is independent of length for the long bridges. Moreover, the asymmetry is larger in the resonant case, in which the site energies of the D, B and A wires are equal, compared to the off-resonant case where the B wire site energy is different from the D and A site energies. These results suggest that ET yield asymmetries may be used to distinguish between resonant and superexchange charge-transfer mechanisms. Moreover, the time dependent calculations indicate that the yield asymmetry increases as the D wire lifetime shortens.

In the steady-state analysis of a donor wire that is coupled directly to an acceptor wire (the DA system), the direction of current on D is transferred to A. In this case, we address the asymmetry in the left and right currents on the A wire. This calculated asymmetry increases with the number of links between the D and A wires and then saturates near 1. In the steady-state analysis of the indirect transfer (the DBA system), we address the asymmetry in total charge transferred from D to A with respect to the direction of the driving current on D. In a similar manner to the case of direct transfer, this asymmetry increases with the number of links between the D and B wires and then

saturates near 1. These large asymmetry factors in the steady-state approach indicate substantial current transfer in both the direct and the bridge-assisted transfers. This calculated asymmetry in the total charge transfer in the case of the DBA system damps exponentially with the site energy of the bridge as transport enters the off-resonance regime.

For both time-dependent and steady-state models, coherent dephasing is taken into account by phenomenological terms in the off diagonal time derivatives of the density matrix elements that appears in the Liouville dynamics. In the time dependent model, increasing the donor or bridge decoherences decreases the yield asymmetry and eventually destroys it only for unphysical large dephasing constants. Ina similar manner, in the steady- state analysis, both the asymmetry in the left and right currents (in the DA system) and the asymmetry in the total charge transferred from D to A (in the DBA system) drop with increasing dephasing. As in the time dependent case, the effect of current transfer in the steady-state approach persists up to relatively large values of dephasing rates.

The time-dependent and steady-state models reviewed here can also be used to analyze the current transfer in a setup of a ring molecule attached to a current carrying molecular wire. In this setup, the current in the linear wire would drive a circular current in the ring molecule that may be detected by its magnetic field [45].

**Acknowledgements.**

This research was supported by the National Science Foundation (CHE-1012357, DNB), the Israel Science Foundation, the German-Israel Foundation and the ERC and the US-Israel Binational Science Foundation (AN), the University of Cyprus (SSS) and the Israel Minisry of Science for a fellowship received under the program for Progressing Women in Science (VBM).

# References

1. Marcus RA, Sutin N (1985) Biochim Biophys Acta 811:265
2. Jortner J, Ratner MA (1997) Molecular Electronics. Oxford: Blackwell Science
3. Kuznetsov AM, Ulstrup J (1999) Electron Transfer in Chemistry and Biology. Chichester, UK: Wiley
4. Jortner J, Bixon M (eds) (1999) Electron Transfer: From Isolated Molecules to Biomolecules. Adv. Chem. Phys. Ser. 106-107. New York: Wiley Interscience

5. May V, Kuhn O (2000) Charge and Energy Transfer Dynamics in Molecular Systems. Berlin: Wiley-VCH
6. Balzani V (ed) (2001) Electron Transfer in Chemistry, Vols 1-5. Weinheim: Wiley-VCH
7. Nitzan A (2006) Chemical Dynamics in Condensed Phases. Oxford: Oxford Univ. Press
8. Skourtis SS, Waldeck DH, Beratan DN (2010) Annu Rev Phys Chem 71:461
9. Beratan DN, Skourtis SS, Balabin IA, Balaeff B, Keinan S, Venkatramani R, Xiao D (2009) Acc Chem Res 42:1669
10. Hod O, Rabani E, Baer R (2006) Acc Chem Res 39:109
11. Galperin M, Nitzan A (2005) Phys Rev Lett 95:206802
12. Galperin M, Nitzan A (2006) J Chem Phys 124:234709
13. Pfeifer T (2006) Nature Physics 2:297
14. Silberberg Y (2004) Nature 430:624
15. Marangos JP (2005) Nature 435:435
16. Hentschel M, Kienberger R, Spielmann Ch, Reider GA, Milosevic N, Brabec T, Corkum P, Heinzmann U, Drescher M, Krausz F (2001) Nature 414:509
17. Niikura H, Légaré F, Hasbani R, Bandrauk AD, Yu. Ivanov M, Villeneuve DM, Corkum PB (2002) Nature 417:917
18. Drescher M, Hentschel M, Kienberger R, Uiberacker M, Yakovlev V, Scrinzi A, Westerwalbesloh Th, Kleineberg U, Heinzmann U, Krausz F (2002) Nature 419:803
19. Niikura H, Légaré F, Hasbani R, Yu Ivanov M, Villeneuve DM, Corkum PB (2003) Nature 421:826
20. Itatani J, Levesque J, Zeidler D, Niikura H, Pépin H, Kieffer JC, Corkum PB, Villeneuve PB (2004) Nature 432:867
21. Kienberger R, Goulielmakis E, Uiberacker M, Baltuska A, Yakovlev V, Bammer F, Scrinzi A, Westerwalbesloh Th, Kleineberg U, Heinzmann U, Drescher M, Krausz F (2004) Nature 427:817
22. Goulielmakis E, Uiberacker M, Kienberger R, Baltuska A, Yakovlev V, Scrinzi A, Westerwalbesloh Th, Kleineberg U, Heinzmann U, Drescher M, Krausz F (2004) Science 305:1267
23. Suzuki T, Minemoto S, Kanai T, Sakai H (2004) Phys Rev Lett 92:133005
24. Brixner T, Krampert G, Pfeifer T, Selle R, Gerber G, Wollenhaupt M, Graefe O, Horn C, Liese D, Baumert T (2004) Phys Rev Lett 92:208301

25. Itatani J, Zeidler D, Levesque J, Spanner M, Villeneuve DM, Corkum PB (2005) Phys Rev Lett 94:123902
26. Kanai T, Minemoto S, Sakai H (2005) Nature 435:470
27. Mauritsson J, Johnsson P, Mansten E, Swoboda M, Ruchon T, L'Huillier A, Schafer KJ (2008) Phys Rev Lett 100:073003
28. Niikura H, Villeneuve DM, Corkum PB (2005) Phys Rev Lett 94:083003
29. Barth I, Manz J, Serrano-Andrés L (2008) Chem Phys 347:263;
30. Barth I, Manz J, Shigeta Y, Yagi K (2006) J Am Chem Soc 128:7043
31. Barth I, Manz J, (2006) Angew Chem Int Ed 45:2962
32. Nobusada K, Yabana K (2007) Phys Rev A 75:032518
33. Lazzerreti P (2000) Prog Nucl Mag Res Sp 36:1-88
34. Steiner E, Fowler P (2001) W J Phys Chem A 105:9553
35. Steiner E, Soncini A, Fowler P (2006) W J Phys Chem A 110:12882
36. Ray K, Ananthavel SP, Waldeck DH, Naaman R (1999) Science 283:814
37. Wei JJ, Schafmeister C, Bird G, Paul A, Naaman R, Waldeck DH (2006) J Phys Chem B 110:1301
38. Skourtis SS, Beratan DN, Naaman R, Nitzan A, Waldeck DH (2008) Phys Rev Lett 101:238103
39. Ben-Moshe V, Nitzan A, Skourtis SS, Beratan DN (2010) J Phys Chem C 114:8005 Ben-Moshe V (2009) Calculations of Electronic Conduction Properties of Molecular Junctions. PhD Thesis, Tel Aviv University
40. Güdde J, Rohleder M, Meier T, Koch SW, Höfer U (2007) Science 318:1287
41. Naaman R, Sanche L (2007) Chem Rev 107:1553
42. Segal D, Nitzan A (2001) Chem Phys 268:315
43. Segal D, Nitzan A (2002) Chem Phys 281:235
44. Solomon GC, Andrews DQ, Hansen T, Goldsmith RH, Wasielewski MR, Duyne RPV, Ratner MA (2008) J Chem Phys 129:054701; Andrews DQ, Solomon DC, Goldsmith RH, Hansen T, Wasielewski MR, Duyne RPV, Ratner MA (2008) J Phys Chem C 112:16991; Ke SH Yang, WT Baranger, HU (2008) Nano Lett 8:3257; Begemann G, Darau D, Donarini A, Grifoni M (2008) Phys Rev B 77:201406; Donarini A, Begemann G, Grifoni M (2009) Nano Lett 9:2897; Xiao DQ, Skourtis SS, Rubtsov IV, Beratan DN (2009) Nano Lett 9:1818
45. Ernzerhof M, Bahmann H, Goyer F, Zhuang M, Rocheleau PJ (2006) Chem Theory Comput 2:1291